coatings

MDPI

Article

Phase Stability and Mechanical Properties of the Monoclinic, Monoclinic-Prime and Tetragonal $REMO_4$ (M = Ta, Nb) from First-Principles Calculations

Wenhui Xiao, Ying Yang, Zhipeng Pi and Fan Zhang *

School of Materials Science and Engineering, Xiangtan University, Xiangtan 411105, China; a18207320474@163.com (W.X.); 18216175931@163.com (Y.Y.); pizhipengmath@163.com (Z.P.)
* Correspondence: zhangfan15@xtu.edu.cn

Abstract: $YTaO_4$ and the relevant modification are considered to be a promising new thermal barrier coating. In this article, phase stability and mechanical properties of the monoclinic (M), monoclinic-prime (M′), and tetragonal (T) $REMO_4$ (M = Ta, Nb) are systematically investigated from first-principles calculations method based on density functional theory (DFT). Our calculations show that M′-$RETaO_4$ is the thermodynamically stable phase at low temperatures, but the stable phase is a monoclinic structure for $RENbO_4$. Moreover, the calculated relative energies between M (or M′) and T phases are inversely proportional to the ionic radius of rare earth elements. It means that the phase transformation temperature of M′→T or M→T could decrease along with the increasing ionic radius of RE^{3+}, which is consistent with the experimental results. Besides, our calculations exhibit that adding Nb into the M′-$RETaO_4$ phase could induce phase transformation temperature of M′→M. Elastic coefficient is attained by means of the strain-energy method. According to the Voigt–Reuss–Hill approximation method, bulk modulus, shear modulus, Young's modulus, and Poisson's ratio of T, M, and M′ phases are obtained. The B/G criterion proposed by Pugh theory exhibits that T, M, and M′ phases are all ductile. The hardness of $REMO_4$ (M = Ta, Nb) phases are predicted based on semi-empirical equations, which is consistent with the experimental data. Finally, the anisotropic mechanical properties of the $REMO_4$ materials have been analyzed. The emerging understanding provides theoretical guidance for the related materials development.

Keywords: phase stability; mechanical properties; modification of $YTaO_4$; lanthanides; first-principles calculations

check for updates

Citation: Xiao, W.; Yang, Y.; Pi, Z.; Zhang, F. Phase Stability and Mechanical Properties of the Monoclinic, Monoclinic-Prime and Tetragonal $REMO_4$ (M = Ta, Nb) from First-Principles Calculations. *Coatings* **2022**, *12*, 73. https://doi.org/10.3390/coatings12010073

Received: 21 November 2021
Accepted: 28 December 2021
Published: 8 January 2022

1. Introduction

The rare-earth tantalate and niobates with the formula $REMO_4$ (M = Ta, Nb) have attracted increasing attention due to their wide application, such as biomedicine, military technology, aerospace, remote sensing, and laser [1]. Moreover, $YTaO_4$ and the relevant modification are extensively investigated and supposed to be promising thermal barrier coatings (TBCs) [2–4] due to high phase stability, good mechanical properties, and thermal conductivity. Because of a ferroelastic toughening mechanism similar to the familiar ZrO_2-8 mol%$YO_{1.5}$ (8YSZ) materials, the high-temperature fracture toughness of $YTaO_4$ is very well [5]. It is well known that $YTaO_4$ has three different crystalline structures, such as monoclinic phase (M, space group I2/a), tetragonal phase (T, space group I41/a), and monoclinic-prime phase (M′, space group P2/a). The high-temperature phase transition is a second-order and displacive transformation when the equilibrium tetragonal (T) transited to the monoclinic (M) $YTaO_4$ phase [6]. Although yttrium tantalate has more superior advantages than YSZ, it still has some shortcomings as a new thermal barrier coating. To improve the properties of the yttrium tantalate, doping and modifying are important.

In the periodic table of elements, yttrium and lanthanides belong to the same group of elements and have similar outermost electronic structures, so $YTaO_4$ can be doped with

lanthanides to change their properties. Therefore, it is of great significance to systematically study the influence of doping of lanthanide on the mechanical and thermal properties of $YTaO_4$. Up to now, a lot of experimental researches on $RETaO_4$ (RE = La, Nd, Gd, Dy, Yb) have been conducted. The mechanical properties of the M phase are found to be better than M′ phase, so it is necessary to stabilize the yttrium tantalate as the M phase below the phase transition temperature. It is studied that the $YTaO_4$ would be stabilized as an M phase when doping 15–30 mol % Nb into $YTaO_4$ materials at 1473 K [7]. It is discovered that the dopant of rare earth elements (Nd, Gd, Dy, Eu, Er, Lu, and Yb) can reduce the thermal conductivity of yttrium tantalate materials [8]. Besides, the mechanical properties and plasticity of $RETaO_4$ (RE = Nd, La, Sm, Gd, Eu, Dy) materials are found to change regularly and become worse and worse with the decrease of atomic radius [9]. In general, yttrium tantalate materials modified by rare earth elements have many advantages, such as great mechanical properties, better thermal stability, and a larger thermal expansion coefficient [10]. Therefore, understanding the doping effects of rare earth elements and Nb on $YTaO_4$ and its phase stability and mechanical properties are significant.

The main purpose of the present work is to systematically investigate the phase stability and mechanical properties of M-, T-, and M′-$REMO_4$ (RE = La, Nd, Gd, Dy, Y; M = Ta, Nb) phases by the first-principles calculation method. Phase stabilities of T-, M-, and M′-$RETaO_4$ or $RENbO_4$ along with the various rare earth elements are studied by comparing their calculated free energies using density functional theory (DFT), and then doping effects of rare earth elements or Nb on $YTaO_4$ are discussed. Elastic stiffness coefficient and elastic flexibility coefficient are attained by means of the strain-energy method. Bulk modulus, Young's modulus, shear modulus, Poisson's ratio, and hardness of T-, M-, and M′-$REMO_4$ (RE = La, Nd, Gd, Dy, Y; M = Ta, Nb) are obtained according to the Voigt–Reuss–Hill approximation method. The B/G criterion proposed by Pugh theory is used to analyze the ductility and brittleness of $REMO_4$ phases. Finally, the anisotropic mechanical properties of the $REMO_4$ materials have been analyzed. It is hoped that the regularity of the $YTaO_4$ materials doped by rare-earth elements or Nb can be determined through first-principles calculations and provide theoretical guidance for the related technological applications.

2. Methods

To theoretically investigate the effect of dopants on the relative stability and mechanical properties of $REMO_4$ (M = Ta, Nb) phases, the first-principles calculations based on density functional theory (DFT) were carried out as implemented in the Vienna Ab-Initio Simulation Package (VASP) [11,12]. The electron-ion interactions were described through projector augmented wave (PAW) [13] and the exchange-correlation functional was constructed by the generalized gradient approximation (GGA) proposed by Perdew–Burke–Ernzerhof (PBE) [14]. The energy cut-off is 550 eV and the converge total energy is less than 1.0 meV/atom. The conjugate gradient method was chosen to relax the structure of atomic positions, cell volumes, and cell shapes. When the residual forces are less than 0.02 eV/Å, the structural relaxations cease. The tetrahedron smearing method with Blochl corrections was used to perform the final self-consistent static calculations [15], and then obtain more accurate energy. For the computation of doping effects of Nb, supercells including 96 atomic sites are used for all structures. A $2 \times 1 \times 2$ supercell is used for the M phase, a $2 \times 2 \times 2$ supercell is used for the M′ phase, and a $2 \times 2 \times 1$ supercell is used for the T phase. To model the doping concentration of 25%, 50%, 75%, we choose 4, 8, and 12 Nb atoms and replace the same amount of Ta atoms in supercells, respectively. Taking $YTaO_4$ as an example, the structures of M, M′, and T phases are listed in Figure 1.

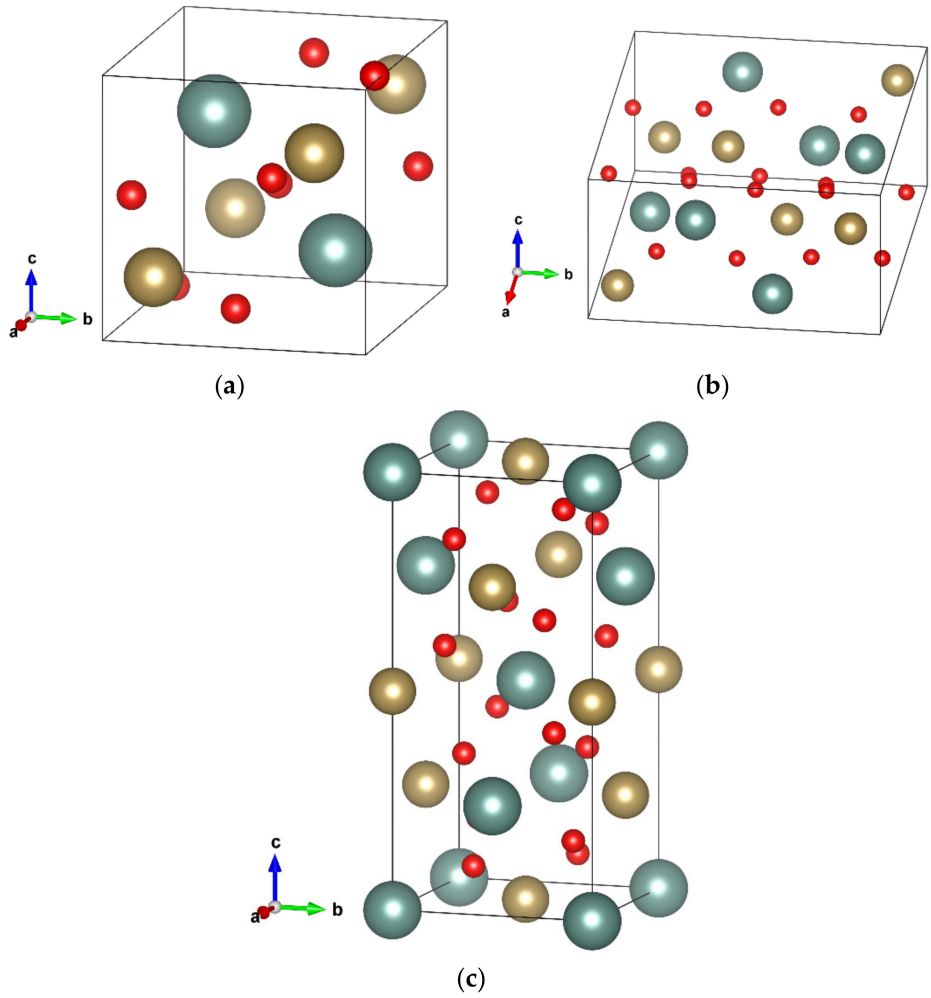

Figure 1. The crystal structures of M, M′, and T phases are listed: The atom of the dark green color is Y; the yellow color is Ta, and the red color is O. (**a**) M′; (**b**) M; (**c**) T.

Elastic Constants

In this work, first-principles calculations are used to calculate the mechanical properties of T-RETa(Nb)O_4, M′-RETa(Nb)O_4, and M-RETa(Nb)O_4 phases). When a very small strain was imposed on the equilibrium crystal, it would exhibit elastic deformation. The strain and stress can be expressed as:

$$\sigma_{ij} = \frac{1}{V_0}\left[\partial E(V,\varepsilon)/\partial\varepsilon_{ij}\right]_{\varepsilon=0} \tag{1}$$

According to the generalized Hooke's law, the elastic constants can be defined as the second derivative of the total energy E (V, ε) to strain,

$$C_{ijkl} = \frac{\partial\sigma_{ij}}{\partial\varepsilon_{kl}} = \frac{1}{V_0}\left[\frac{\partial^2 E(V,\varepsilon)}{\partial\varepsilon_{ij}\partial\varepsilon_{kl}}\right]_{\varepsilon=0} \tag{2}$$

The total energy of a crystal could be expanded using the following Taylor form:

$$E(V,\varepsilon_{ij}) = E(V_0,0) + V_0\sum_{ij}\sigma_{ij}\varepsilon_{ij} + \frac{V_0}{2}\sum_{ijkl}C_{ijkl}\varepsilon_{ij}\varepsilon_{kl} + \ldots \tag{3}$$

where E (V_0, 0) is the total energy and V_0 is the volume of the unstrained system. As shown in the above formula, the strain tensors subscripts (ij, kl) are explained in the Voigt notation

scheme (11 = 1, 22 = 2, 33 = 3, 23 = 4, 31 = 5, and 12 = 6) [16]. Before and after the different strains, the total energy variation can be fit by using a multinomial formula. Then we can obtain a secondary coefficient. In this work, 8 distortions to the lattice cell are applied to the lattice cell, and the relaxation in all the strained unit cells was finished when the total energy was converged to less than 1.0 meV/atom.

The Young's modulus (Y), shear modulus (G or μ), bulk modulus (B) and Poisson's ratio (ν) of the polycrystalline crystal were acquired from independent single-crystal elastic constants. In general, the polycrystalline modulus can be approximately assessed by two methods (the Voigt method and the Reuss method) [17,18], and they are expressed as:

$$9B_V = C_{11} + C_{22} + C_{33} + 2(C_{12} + C_{13} + C_{23}) \quad (4)$$

$$\frac{1}{B_R} = (S_{11} + S_{22} + S_{33}) + 2(S_{12} + S_{13} + S_{23}) \quad (5)$$

$$15G_V = (C_{11} + C_{22} + C_{33}) - (C_{12} + C_{13} + C_{23}) + 3(C_{44} + C_{55} + C_{66}) \quad (6)$$

$$15/G_R = 4(S_{11} + S_{22} + S_{33}) - 4(S_{12} + S_{13} + S_{23}) + 3(S_{44} + S_{55} + S_{66}) \quad (7)$$

where the subscripts R and V represent the Reuss and Voigt. The elastic compliance matrices were described as $\{S_{ij}\}$, which is obtained by the inverse matrix of the elastic constant $\{C_{ij}\}^{-1}$. The Voigt–Reuss–Hill approximation [19], which was obtained by the average of Voigt and Reuss bounds, was considered as the best estimation of the polycrystalline elastic modulus. It was indicated as:

$$B_H = (B_V + B_R)/2 \; G_H = (G_V + G_R)/2 \quad (8)$$

In addition, the Poisson's ratio and the polycrystalline elastic modulus can be obtained using the following relationship:

$$Y_H = \frac{9B_H G_H}{3B_H + G_H} \; \nu_H = \frac{3B_H - 2G_H}{2(3B_H + G_H)} \quad (9)$$

3. Results

3.1. Structural Properties and Thermodynamic Properties

In the present work, structure relaxations of T, M, and M′-$REMO_4$ (RE = Y, Dy, Gd, Nd, La; M = Ta, Nb) phases were performed. The crystal structures of M-, M′-$RENbO_4$, and $RETaO_4$ phases both belong to the monoclinic crystal structure, and the T phase is the tetragonal crystal. Tables 1 and 2 list the calculated information of the crystal lattice at 0 K and the experimental data [20,21]. Our calculated results are consistently consistent with the experimental values. Both the calculations and experiments show that the small rare earth atom in $RETaO_4$ or $RENbO_4$ phases have small volumes. Besides, the β angle of the M phase and M′ phase also gradually decrease with the decrease of the atomic radius of RE^{3+}.

Figure 2a-j show the total energies for T, M, and M′-$REMO_4$ (RE = Y, Dy, Gd, Nd, La; M = Ta, Nb) phases, which are changed with a function of volume at 0 K. The equation of state (EOS) is used to fit the energy-volume. As we know, there are three crystalline structures in $RETaO_4$ materials, and they are monoclinic phase (M, space group I2/a), tetragonal phase (T, space group I41/a), and monoclinic-prime phase (M′, space group P2/a). At the high temperature, the stable phase is the T-$RETaO_4$, and it can transform to the M phase through a displacive transformation of T→M. However, the true equilibrium phase at low temperature is the M′ phase, which only can be obtained by means of synthesizing below the temperature of T→M transformation. Therefore, the M′ phase is the low-temperature phase of the $RETaO_4$ materials. As shown in Figure 2a–j, our calculated results show that the M phase and T phase are both less stable than the M′ phase. It implies that the M phase is metastable and the M′ phase is stable at low temperatures. This is consistent with the experimental results [22]. For $RENbO_4$ phases, only low-temperature M and high-temperature T phases are existent in the literature. As for comparisons, the M′-$RENbO_4$ structures are also calculated in this work. In Figure 2a–j, our calculations

exhibit that the total energy of the M-$RENbO_4$ phase is larger than that of the M′ phase, so the M phase is a true equilibrium phase at low temperature. This is consistent with the experimental results [22] that M′-$RENbO_4$ crystalline structures do not exist in the $RENbO_4$ phases.

Table 1. Calculated lattice parameters (Å) of M-, M′-, and T-$RETaO_4$ phases along with the experimental data.

Phase	Abbr.	Group	a	b	c	β	Remark
$YTaO_4$	T	I41/a	5.23	5.23	11.06		cal
	M′	P2/a	5.15	5.53	5.34	96.40°	cal
			5.26	5.43	5.08	96.08°	exp [20]
	M	I2/a	5.362	11.071	5.093	95.58°	cal
			5.24	10.89	5.06	95.31°	exp [21]
$DyTaO_4$	T	I41/a	5.24	5.24	11.06		cal
	M′	P2/a	5.34	5.52	5.15	96.58°	cal
		P2/a	5.32	5.48	5.14	96.52°	exp [20]
	M	I2/a	5.36	11.07	5.10	95.51°	cal
		I2/a	5.35	10.97	5.06	95.6°	exp [21]
$GdTaO_4$	T	I41/a	5.27	5.27	11.17		cal
	M′	P2/a	5.38	5.55	5.19	96.75°	cal
		P2/a	5.36	5.52	5.17	96.66°	exp [20]
	M	I2/a	5.41	11.15	5.11	95.53°	cal
		I2/a	5.41	11.07	5.08	95.6°	exp [21]
$NdTaO_4$	T	I41/a	5.37	5.37	11.48		cal
	M′	P2/a	5.47	5.66	5.28	96.83°	cal
		P2/a	5.43	5.60	5.24	96.77°	exp [20]
	M	I2/a	5.55	11.40	5.17	95.47°	cal
		I2/a	5.51	11.23	5.11	95.7°	exp [21]
$LaTaO_4$	T	I41/a	5.44	5.44	11.69		cal
	M′	P2/a	5.52	5.77	5.34	96.75°	cal
	M	I2/a	5.65	11.57	5.19	95.63°	cal
	nM	P21/c	7.77	5.59	7.86	101.13°	cal
		P21/c	7.76	5.58	7.81	101.53°	exp [20]

Table 2. Calculated lattice parameters (Å) of M-, M′-, and T-$RENbO_4$ phases along with the experimental data.

Phase	Abbr.	Group	a	b	c	β	Remark
$YNbO_4$	T	I41/a	5.25	5.25	11.08		cal
	M′	P2/a	5.11	5.45	5.29	96.44°	cal
	M	I2/a	5.31	10.97	5.07	94.42°	cal
		I2/a	5.29	10.94	5.07	94.32°	exp [21]
$DyNbO_4$	T	I41/a	5.25	5.25	11.11		cal
	M′	P2/a	5.15	5.49	5.37	95.77°	cal
	M	I2/a	5.34	11.11	5.15	93.89°	cal
		I2/a	5.32	11.00	5.07	94.34°	exp [21]
$GdNbO_4$	T	I41/a	5.29	5.29	11.22		cal
	M′	P2/a	5.18	5.53	5.41	95.85°	cal
	M	I2/a	5.38	11.21	5.18	93.74°	cal
		I2/a	5.37	11.09	5.11	94.37°	exp [21]
$NdNbO_4$	T	I41/a	5.38	5.38	11.53		cal
	M′	P2/a	5.27	5.66	5.50	95.98°	cal
	M	I2/a	5.47	11.51	5.29	92.42°	cal
		I2/a	5.47	11.28	5.14	94.32°	exp [21]
$LaNbO_4$	T	I41/a	5.45	5.45	11.74		cal
	M′	P2/a	5.33	5.76	5.55	95.86°	cal
	M	I2/a	5.57	11.53	5.20	94.40°	exp [21]

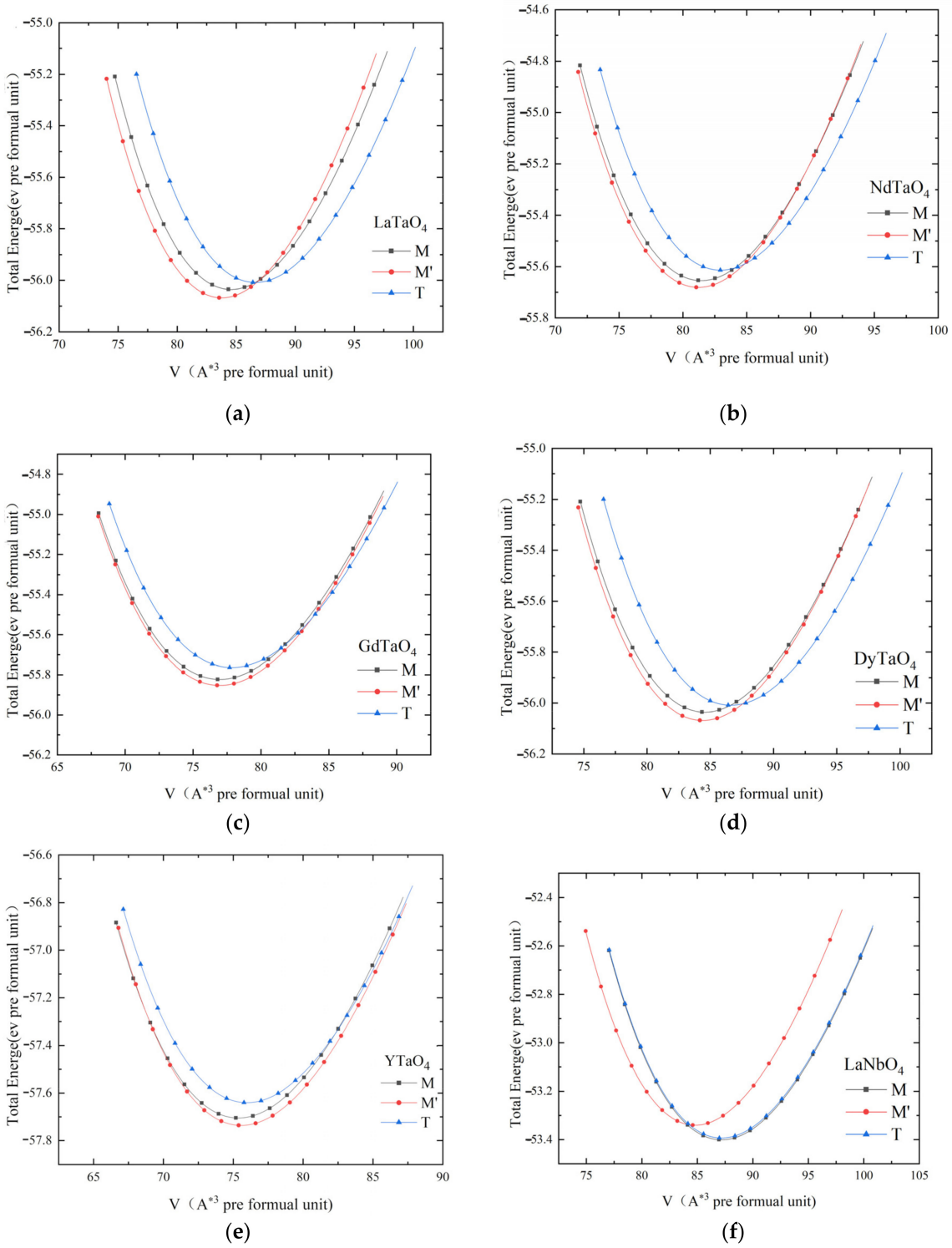

Figure 2. *Cont.*

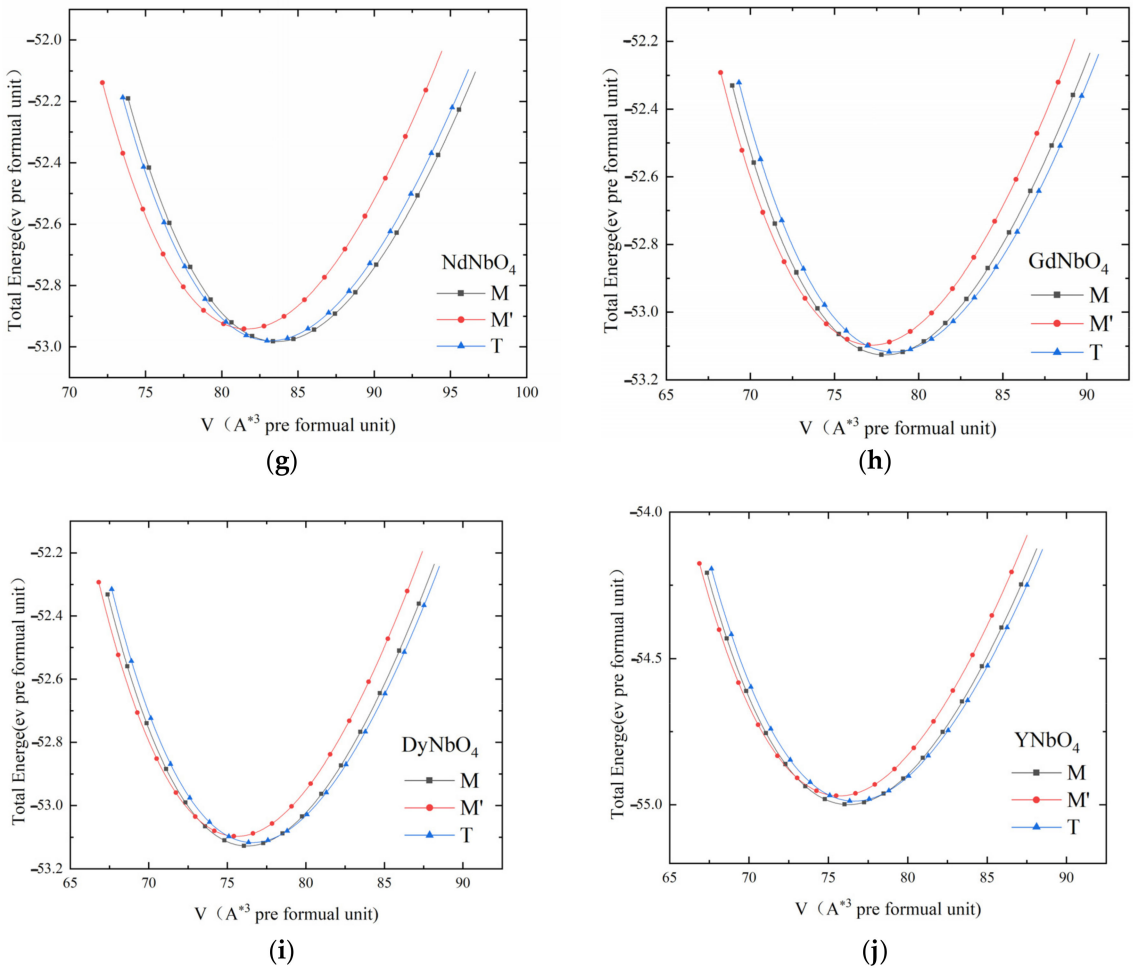

Figure 2. (**a**–**j**). Calculated total energies as a function of volume of T- and M-$RENbO_4$ phases and M′-$RENbO_4$ phase: (**a**) $LaTaO_4$; (**b**) $NdTaO_4$; (**c**) $GdTaO_4$; (**d**) $DyTaO_4$; (**e**) $YTaO_4$; (**f**) $LaNbO_4$; (**g**) $NdNbO_4$; (**h**) $GdNbO_4$; (**i**) $DyNbO_4$; (**j**) $YNbO_4$.

Figure 3 presents the relative energies ($\Delta E_{M'\to T \text{ or } M\to T}$) of M′- or M-$REMO_4$ with respect to that of T-$REMO_4$ for different rare-earth atoms of Y, Dy, Gd, Nd, and La. It is obvious that the relative energies are inversely proportional to the ionic radius of RE^{3+}. The Gibbs free energy difference of M′→T or M→T phase transformation $\Delta G_{M'\to T \text{ or } M\to T}$ can be expressed as $\Delta H_{M'\to T \text{ or } M\to T}$ -$\Delta S_{M'\to T \text{ or } M\to T}$*T. If the differences in the enthalpy ΔH (≈ΔE) and entropy ΔS are assumed to be substantially unchanged 4 [23] and ΔS is supposed to be similar for the different rare-earth dopants, phase transformation temperature of M′→T or M→T may increase with the decreasing ionic radius of RE^{3+} for Y, Dy, Gd, Nd, and La. This is consistent with the measured results using a high-temperature X-ray diffractometer by Stubičan [24]. Figure 3 presents the comparison of the experimental transformation temperature and our calculated relative energies, which indicates that the relative energies and transformation temperature decrease with the increase of the rare earth ionic radius.

As M′ and M are the stable phases at the low temperature for the $RETaO_4$ and $RENbO_4$ structures, respectively, adding the Nb element into the M′-$RETaO_4$ phase should induce phase transformation of M′→M at the appropriate compositions. Based on the first-principles calculations, phase transformation of M′→M induced by the dopant of Nb is studied in this work. Figure 4 presents our calculated relative energies ($\Delta E_{M'\to M}$) of M′-$RETa_xNb_{1-x}O_4$ (x = 0.25, 0.5, 0.75) with respect to that of M-$RETa_xNb_{1-x}O_4$ (x = 0.25, 0.5, 0.75) for different rare-earth atoms of Y, Dy, Gd, Nd, and La. When $\Delta E_{M'\to M} > 0$, this means that M′ is thermodynamically stable. Conversely, when $\Delta E_{M'\to M} < 0$, it implies that

M is thermodynamically more stable than M′. In Figure 4, the M′-$RETa_xNb_{1-x}O_4$ phase will transform into the M-$RETa_xNb_{1-x}O_4$ phase when the composition of the dopant Nb is about 0.5. It is worth mentioning that our calculated results are related to the phase transformation at 0 K, and transformation composition may decrease at the high temperature.

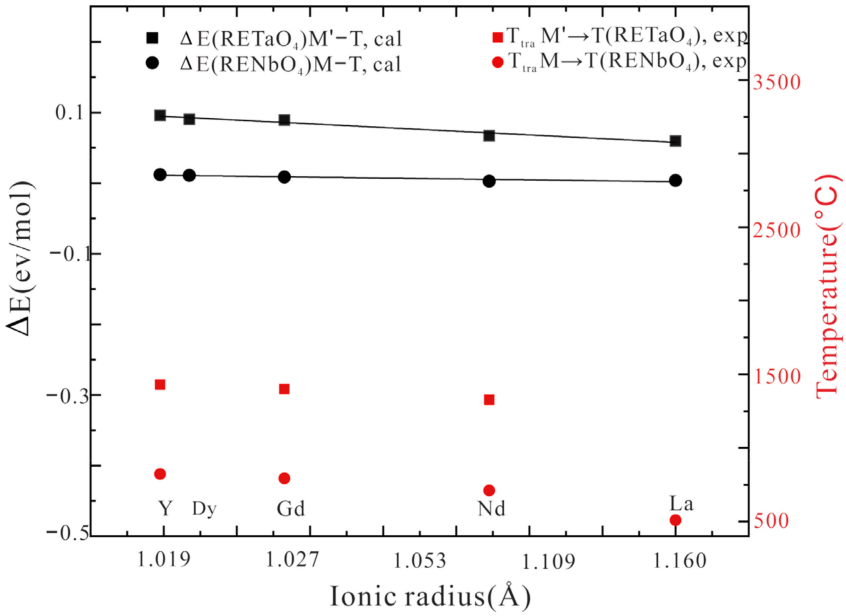

Figure 3. Comparison of the experimental transformation temperature and our calculated relative energies for different rare-earth atoms of Y, Dy, Gd, and Nd.

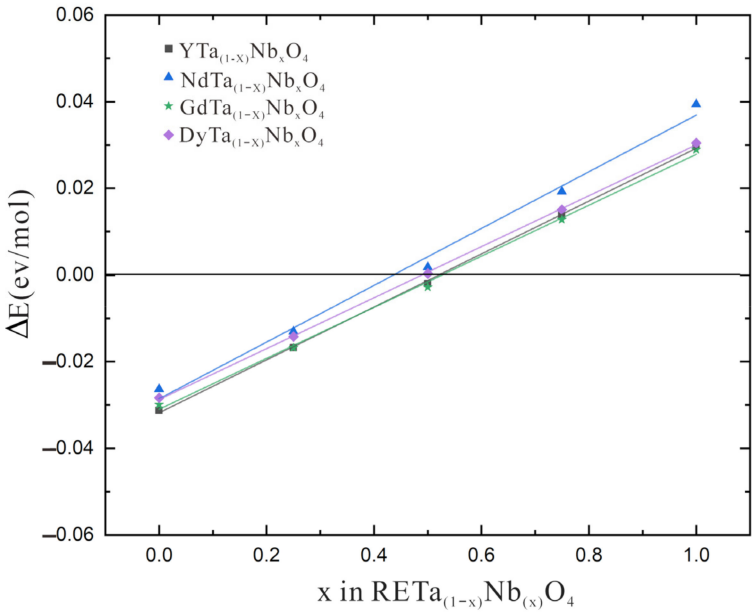

Figure 4. Calculated relative energies ($\Delta E_{M'\rightarrow M}$) of M′-$RETa_xNb_{1-x}O_4$ (x = 0.25, 0.5, 0.75) with respect to that of M-$RETa_xNb_{1-x}O_4$ (x = 0.25, 0.5, 0.75) for different rare earth atoms of Y, Dy, Gd, Nd.

3.2. Mechanical Properties

The calculated elastic constants are listed in Tables 3–5. Because the T-$YTaO_4$ phase is tetragonal, C_{11}, C_{12}, C_{13}, C_{33}, C_{44}, and C_{66} can be determined through six deformation modes [25]. As M′-$YTaO_4$ and M-$YTaO_4$ phases are both monoclinic, the thirteen independent elastic constants can be obtained by applying thirteen distortions [26]. The total energies are varied before and after a set of different strains (±1%, ±2%, ±3%, and ±4%), and the elastic constants were calculated by the quadratic coefficients. For stable structures,

the elastic constants need to meet the mechanical stability criterion [27]. The monoclinic system criteria are $C_{11} > 0$, $C_{22} > 0$, $C_{33} > 0$, $C_{44} > 0$, $C_{55} > 0$, $C_{66} > 0$, $C_{44}C_{66} - 2C_{46} > 0$, $C_{11} + C_{22} + C_{33} + 2(C_{12} + C_{13} + C_{23}) > 0$, $C_{22} + C_{33} - 2C_{23} > 0$. The tetragonal system criteria are $C_{11} > 0$, $C_{33} > 0$, $C_{44} > 0$, $C_{66} > 0$, C_{11}-$C_{12} > 0$, $C_{11} + C_{33} - 2C_{13} > 0$, $2C_{11}+C_{33}+2C_{12}+4C_{13} > 0$. All $RETaO_4$ (RE = La, Nd, Gd, Dy) and $RENbO_4$ (RE = La, Nd, Gd, Dy) materials meet the criterion of mechanical stability, and the structures are stable.

Table 3. Elastic constants C_{ij} for the M phases of $RETaO_4$ and $RENbO_4$. All quantities are in GPa.

M-$RETaO_4$	C_{11}	C_{22}	C_{33}	C_{44}	C_{55}	C_{66}	C_{12}	C_{13}	C_{23}	C_{16}	C_{26}	C_{36}	C_{45}
La	217.07	168.49	230.98	43.28	55.86	56.26	61.27	106.50	90.21	25.28	6.27	−13.88	−1.14
Nd	229.36	193.08	255.53	50.63	62.02	67.21	63.53	116.64	98.38	21.92	1.88	−19.63	−2.09
Gd	249.50	212.45	270.47	58.12	61.57	83.45	70.90	131.87	95.84	13.11	−2.83	−20.28	−4.73
Dy	255.11	220.50	275.98	57.91	60.10	88.91	74.01	136.94	94.82	10.69	−4.04	−19.74	−4.96
Y	257.02	221.67	273.37	56.72	57.56	87.77	74.78	135.87	93.11	8.91	−4.74	−19.08	−5.23
M-$RENbO_4$	**C_{11}**	**C_{22}**	**C_{33}**	**C_{44}**	**C_{55}**	**C_{66}**	**C_{12}**	**C_{13}**	**C_{23}**	**C_{16}**	**C_{26}**	**C_{36}**	**C_{45}**
La	171.39	154.27	195.03	30.25	34.82	33.65	63.13	100.72	75.39	34.69	4.56	−23.70	3.09
Nd	157.05	169.74	224.90	29.37	43.43	47.48	49.18	117.27	84.96	45.25	8.44	−23.51	8.18
Gd	195.53	194.15	245.42	42.11	49.75	69.42	64.69	134.61	83.74	29.95	0.79	−22.30	2.39
Dy	205.94	201.75	249.32	45.85	49.62	75.96	68.74	140.48	81.48	25.77	−1.20	−21.93	0.68
Y	202.58	192.94	248.02	44.99	47.80	75.01	65.47	135.69	76.74	25.19	−1.17	−20.13	0.41

Table 4. Elastic constants C_{ij} for the M′ phases of $RETaO_4$ and $RENbO_4$. All quantities are in GPa.

M′-$RETaO_4$	C_{11}	C_{22}	C_{33}	C_{44}	C_{55}	C_{66}	C_{12}	C_{13}	C_{23}	C_{16}	C_{26}	C_{36}	C_{45}
La	238.64	162.73	253.65	52.01	60.31	59.34	86.70	113.51	87.66	16.34	−13.07	9.78	−10.43
Nd	266.93	178.92	271.78	62.93	62.67	66.14	91.90	118.95	90.78	15.35	−14.16	8.47	−9.67
Gd	288.41	176.27	296.06	66.70	59.66	71.33	88.50	119.39	90.73	14.69	−15.78	11.01	−7.09
Dy	296.31	173.88	304.01	67.04	56.06	71.97	84.00	118.53	89.13	14.15	−17.72	11.54	−6.91
Y	290.40	141.65	298.91	64.01	53.08	71.22	74.32	113.46	75.89	11.68	−20.59	10.52	−8.10
M′-$RENbO_4$	**C_{11}**	**C_{22}**	**C_{33}**	**C_{44}**	**C_{55}**	**C_{66}**	**C_{12}**	**C_{13}**	**C_{23}**	**C_{16}**	**C_{26}**	**C_{36}**	**C_{45}**
La	235.54	155.44	220.45	46.37	53.15	47.89	84.43	111.03	84.45	16.31	−6.62	−7.09	−10.34
Nd	258.48	181.92	240.56	53.68	57.23	50.10	91.42	113.48	88.80	17.39	−7.71	−7.47	−9.32
Gd	280.10	189.47	259.83	57.03	57.10	53.72	88.91	110.44	92.54	18.43	−2.49	−3.91	−4.55
Dy	292.68	188.65	271.23	57.82	55.63	55.05	88.54	112.08	96.52	18.88	−0.28	−1.63	−2.45
Y	288.33	181.77	271.43	56.05	53.58	54.05	84.43	110.17	94.51	17.74	−1.31	−1.75	−2.21

Table 5. Elastic constants C_{ij} for the T phases of $RETaO_4$ and $RENbO_4$. All quantities are in GPa.

T-$RETaO_4$	C_{12}	C_{11}	C_{33}	C_{44}	C_{66}	C_{13}	C_{16}
La	124.89	163.70	151.93	29.66	27.52	71.67	113.03
Nd	122.49	194.92	172.31	31.22	28.68	73.87	147.44
Gd	121.73	228.82	192.05	29.00	13.41	74.49	93.62
Dy	120.51	241.46	201.29	27.93	11.56	74.64	148.69
Y	118.20	237.39	198.37	26.25	12.87	71.61	69.08
T-$RENbO_4$	**C_{12}**	**C_{11}**	**C_{33}**	**C_{44}**	**C_{66}**	**C_{13}**	**C_{16}**
La	112.79	169.36	151.35	31.98	34.65	72.74	128.76
Nd	114.62	196.62	170.36	34.74	29.99	75.69	138.65
Gd	115.24	226.54	190.83	33.89	14.65	77.27	159.76
Dy	116.10	239.29	198.93	33.28	9.67	78.08	164.16
Y	111.40	233.13	197.32	31.69	9.17	75.04	146.88

'The polycrystalline elastic mechanical properties, such as shear modulus (G or μ), bulk modulus (B), Young's modulus (Y), and Poisson's ratio (ν) could be obtained through the Voigt and Reuss methods according to the calculated elastic constants. Using energy

considerations, Hill [20] certificated the elastic moduli of the Voigt and Reuss methods are the upper and lower limits of polycrystalline constants. The practical elastic modulus can be estimated by the arithmetic means of these extremes. Generally, the bulk modulus is a measure of resistance to volume change by applied pressure. As seen from Figure 5 and Tables 6–8, the calculated shear modulus and bulk modulus of M-, M′-, T-$RETaO_4$, and $RENbO_4$ (RE = Y, Dy, Gd, Nd, La) is decreased with the increase of the rare-earth atoms, which indicate that the resistance to volume change through applied pressure is eventually lowered. Moreover, the calculated bulk modulus of rare-earth tantalate is regularly larger than and rare-earth niobates. The calculated shear modulus shows a similar trend, which means that the resistance to reversible deformations upon shear stress for $RETaO_4$ and $RENbO_4$ (RE = Y, Dy, Gd, Nd, La) is decreased with the increase of the rare-earth atoms. The ratio between bulk modulus and shear modulus, proposed by Pugh theory [28], can be used to empirically predict the brittleness and ductility of materials. A low B/G ratio is associated with brittleness, and a high value indicates its ductile nature. The empirically critical value which distinguishes ductile and brittle materials is around 1.75. In the present work, the calculated B/G of $REMO_4$ in Figure 6 is larger than 1.75, which means that all $REMO_4$ materials are ductile.

Table 6. Bulk modulus (GPa), shear modulus (GPa), B/G, Young modulus (GPa), Poisson ratio, and Vickers-hardness (Kg·N) for T-$REMO_4$ (M = Ta,Nb) phases.

T-$RETaO_4$	**B**	**G**	**B/G**	**E**	**ν**	**H_v**	**Remake**
La	111.33	29.97	3.71	82.50	0.38	278.11	cal
Nd	120.97	36.28	3.33	98.95	0.36	319.77	cal
Gd	130.55	33.95	3.84	93.74	0.38	270.37	cal
Dy	134.21	33.87	3.96	93.71	0.38	261.17	cal
Y	131.14	33.86	3.87	93.52	0.38	268.04	cal
	128.9	52.7	2.45	139.1	0.32	-	exp [3]
T-$RENbO_4$	**B**	**G**	**B/G**	**E**	**ν**	**H_v**	**Remark**
La	110.57	34.52	3.20	93.80	0.36	333.25	cal
Nd	120.38	38.68	3.11	104.82	0.35	347.78	cal
Gd	130.04	36.34	3.58	99.72	0.37	295.08	cal
Dy	134.24	34.04	3.94	96.69	0.38	262.75	cal
Y	130.41	33.26	3.92	91.97	0.38	263.96	cal

Table 7. Bulk modulus (GPa), shear modulus (GPa), B/G, Young modulus (GPa), Poisson ratio, and Vickers-hardness (Kg·N) for M′-$REMO_4$ (M = Ta,Nb) phases.

M′-$RETaO_4$	**B**	**G**	**B/G**	**E**	**ν**	**H_v**	**Remark**
La	132.73	56.96	2.33	149.48	0.31	481.9	cal
Nd	142.66	64.43	2.21	168.01	0.30	515.73	cal
Gd	144.97	68.23	2.12	176.93	0.30	542.89	cal
Dy	144.00	68.59	2.10	177.04	0.30	550.51	cal
Y	128.67	65.20	2.19	167.34	0.28	588.38	cal
	132.7	66.1	2.01	170.2	0.29	-	exp [3]
M′-$RENbO_4$	**B**	**G**	**B/G**	**E**	**ν**	**H_v**	
La	126.58	50.02	2.53	132.60	0.33	434.37	cal
Nd	138.32	56.44	2.45	149.05	0.32	454.79	cal
Gd	143.03	61.34	2.33	161.00	0.31	484.34	cal
Dy	145.98	62.52	2.33	164.14	0.31	484.391	cal
Y	142.59	61.29	2.33	160.75	0.31	485.32	cal

Table 8. Bulk modulus (GPa), shear modulus (GPa), B/G, Young modulus (GPa), Poisson ratio, and Vickers-hardness (Kg·N) for M-REMO$_4$ (M = Ta,Nb) phases.

M-RETaO$_4$	B	G	B/G	E	ν	H$_v$	Remark
La	122.08	52.80	2.31	138.45	0.32	483.34	cal
Nd	134.00	60.47	2.22	157.69	0.31	512.68	cal
	-	-	-	-	-	641	exp [8]
Gd	145.03	67.75	2.14	175.87	0.31	537.98	cal
	-	-	-	-	-	610	exp [8]
Dy	148.88	69.15	2.15	179.61	0.31	535.20	cal
	-	-	-	-	-	534	exp [8]
Y	148.68	68.32	2.18	177.74	0.30	528.35	cal
	183.7	63.2	2.91	170.1	0.34	378	exp [3]
M-RENbO$_4$	**B**	**G**	**B/G**	**E**	**ν**	**H$_v$**	**Remark**
La	106.00	30.05	3.53	82.38	0.37	286.18	cal
Nd	107.85	39.70	2.72	106.08	0.331	393.53	cal
Gd	129.36	50.99	2.54	135.21	0.33	433.19	cal
Dy	134.53	54.51	2.47	144.08	0.32	449.5	cal
Y	129.95	54.12	2.4	142.57	0.32	463.94	cal

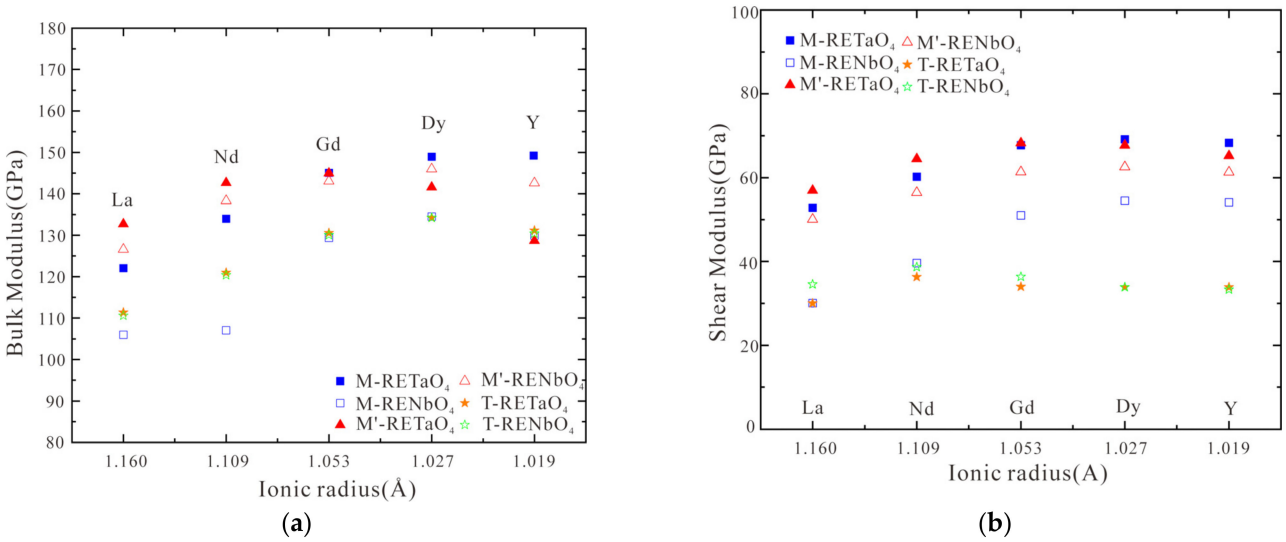

(**a**) (**b**)

Figure 5. Calculated bulk modulus and shear modulus of M-, M′-, T-RETaO$_4$, and RENbO$_4$ along with the ionic radius of RE^{3+}: (**a**) bulk modulus; (**b**) shear modulus.

Young's modulus E can be used to estimate the stiffness of materials. The calculations of M-, M′-, T-RETaO$_4$ or RENbO$_4$ in Figure 7 and Tables 6–8 suggest that Young's modulus is decreased with an increase of the rare-earth atoms, which means that M-, M′-, and T-YTaO$_4$ are the stiffest, and then followed by DyTaO$_4$, GdTaO$_4$, NdTaO$_4$, and LaTaO$_4$. Moreover, our calculated results indicate that RETaO$_4$ is stiffer than RENbO$_4$. Poisson's ratio (ν) is also related to the brittleness and ductility of materials. A compound is considered brittle if the ν is <0.26 [29]. The higher value of Poisson's ratio is, the more ductile the material is. Thus, Tables 6–8 show that all REMO$_4$ materials are ductile. They are in good agreement with the results estimated by the B/G ratio. Besides, the value of Poisson's ratio suggests that the ductility is inversely proportional to the rare earth atom of REMO$_4$ materials, and RENbO$_4$ is more ductile than RETaO$_4$.

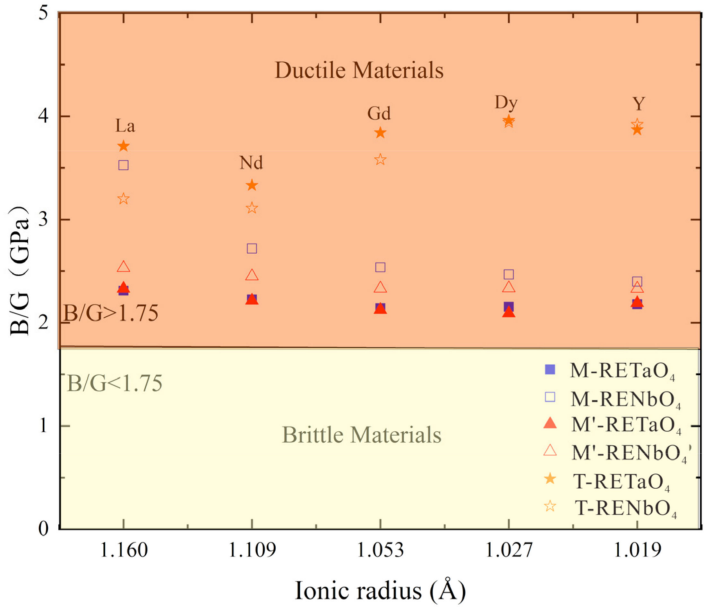

Figure 6. Calculated B/G of $REMO_4$(M = Ta, Nb) along with the ionic radius of RE^{3+}.

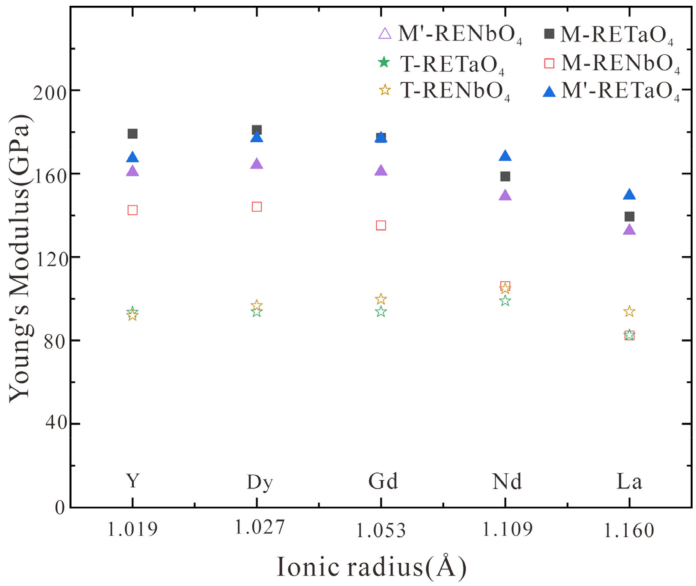

Figure 7. Calculated Young's modulus of M-, M′-, T-$REMO_4$ (M = Ta, Nb) along with the ionic radius of RE^{3+}.

Hardness is a very important mechanical property in applications. Hardness is defined as the resistance of a material to deformation and may be predicted using macroscopic and microscopic models. In this work, we use the semi-empirical equations of hardness proposed by Chen et al. [30] and Tian et al. [31] were used to study the hardness of the $REMO_4$ phases. The equations of these two models are defined as follow:

$$H_V = 2(k^2G)^{0.585} - 3 \quad (10)$$

$$H_V = 0.92k^{1.137}G^{0.708} \quad (11)$$

where k = G/B, G and B are the shear modulus and the bulk, respectively. The obtained hardness of $REMO_4$ phases are shown in Figure 8 and Tables 6–8 presents a comparison between the calculated and experimental results, which exhibits a good consistency. Besides, our calculations suggest that the Vickers hardness of the T phase decreases, and the single-phase gradually increase with the decrease of the atomic radius.

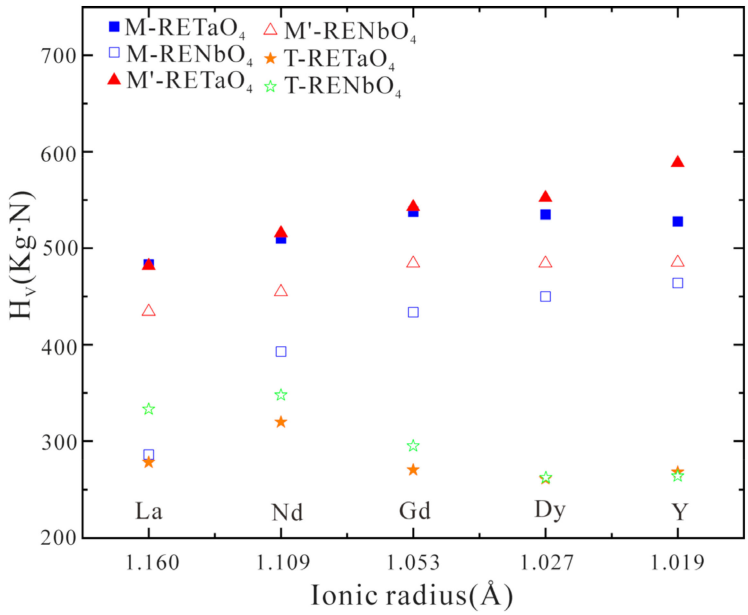

Figure 8. The calculated hardness of $REMO_4$ phases (M = Ta, Nb) along with the ionic radius of RE^{3+}.

The anisotropic mechanical properties of the compounds are very important in applications. Based on the G and B values from Reuss and Voigt, Ranganathan et al. [32] proposed a universal elastic anisotropy index A^U for crystal with any symmetry as shown below:

$$A^U = \frac{5G_{Voigt}}{G_{Reuss}} + \frac{B_{Voigt}}{B_{Reuss}} - 6 \geq 0 \quad (12)$$

A^U is equal to zero when the single crystals are locally isotropic. The extent of single-crystal anisotropy can be expressed by the departure from zero indicates. The highly mechanical anisotropic properties exhibit large discrepancies from zero. The calculated elastic anisotropy is shown in Figure 9. Most values of A^U are lower than 1. The larger the value of A^U is, the stronger the anisotropy of the phase. The M-, M′- and T-$REMO_4$ are anisotropic, and the elastic anisotropy of M and M′ phases is larger than the tetragonal (T) phase.

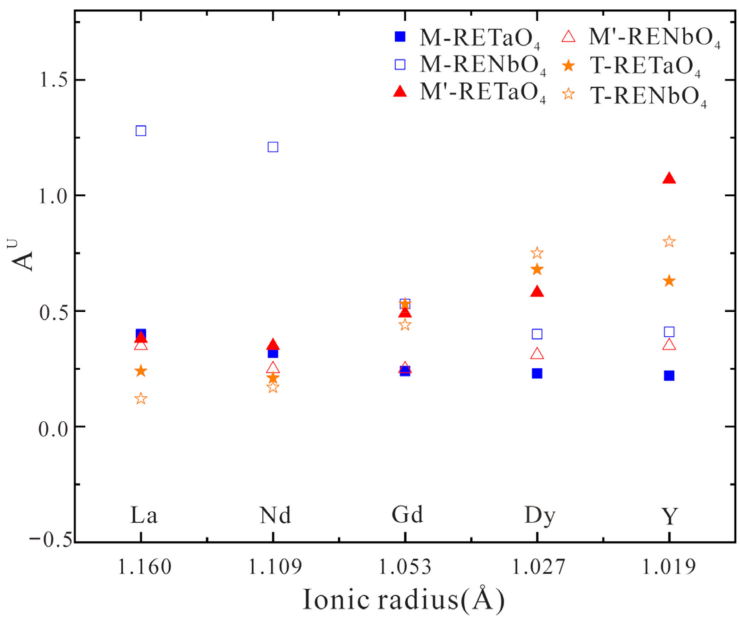

Figure 9. Calculated elastic anisotropy of $REMO_4$ phases (M = Ta, Nb) along with the ionic radius of RE^{3+}.

4. Conclusions

In the present work, phase stability and mechanical properties of $REMO_4$ (RE = La, Nd, Gd, Dy, Y; M = Ta, Nb) are investigated by first-principles calculations. Some conclusions can be found. For $RETaO_4$, the M′ phase is more stable than the M phase at low temperature, and the T phase is only stable at high temperature. For $RENbO_4$, only the M phase is stable at low temperatures. This is consistent with the experimental results. Our calculated relative energies ($\Delta E_{M'\rightarrow T \text{ or } M\rightarrow T}$) of M′- or M-$REMO_4$ with respect to that of T-$REMO_4$ for different rare-earth atoms are inversely proportional to the ionic radius of RE^{3+}. This implies that the phase transformation temperature of M′→T or M→T is decreased with the increase of the rare-earth atoms, which is consistent with the experimental data. Moreover, our calculations exhibit that adding Nb into M′-$RETaO_4$ can induce phase transformation of M′→M, and the doping concentration is about 50%. Besides, the elastic coefficient is attained by means of the strain-energy method. Bulk modulus, Young's modulus, shear modulus, and Poisson's ratio of T-, M-, and M′ phases are obtained according to Voigt-Reuss-Hill approximation, and anisotropic mechanical properties of the $REMO_4$ materials have been calculated. Finally, our calculated B/G exhibits that T-, M-, and M′ phases are all ductile, and the hardness of $REMO_4$ phases are predicted based on semi-empirical equations, which is consistent with the experimental data.

Author Contributions: Investigation, writing—original draft preparation, W.X.; data curation, Y.Y.; funding acquisition, Z.P.; writing—review and editing, funding acquisition, F.Z. All authors have read and agreed to the published version of the manuscript.

Funding: This research was funded by the National Natural Science Foundation of China (No. 51801170 and 11802257), National Postdoctoral Program for Innovative Talents (No. BX20180265), Natural Science Foundation of Hunan Province (No. 2019JJ50570), China Postdoctoral Science Foundation (No. 2019M652786), Research initiation project of Xiangtan University (No. 18QDZ24) and Research foundation of education bureau of Hunan province, No. 21B0163.

Institutional Review Board Statement: Not applicable.

Informed Consent Statement: Not applicable.

Data Availability Statement: Not applicable.

Conflicts of Interest: The authors declare no conflict of interest.

References

1. Voloshyna, O.; Neicheva, S.V.; Starzhinskiy, N.G.; Zenya, I.M.; Gridin, S.S.; Baumer, V.N.; Sidletskiy, O.T. Luminescent and scintillation properties of orthotantalates with common formulae $RETaO_4$ (RE = Y, Sc, La, Lu and Gd). *Meter. Sci. Eng. B* **2013**, *178*, 1491–1496. [CrossRef]
2. Shian, S.; Sarin, P.; Gurak, M.; Baram, M.; Kriven, W.M.; Clarke, D.R. The tetragonal-monoclinic, ferroelastic transformation in yttrium tantalate and effect of zirconia alloying. *Acta Mater.* **2014**, *69*, 196–202. [CrossRef]
3. Feng, J.; Shian, S.; Xiao, B.; Clarke, D.R. First-principles calculations of the high-temperature phase transformation in yttrium tantalate. *Phys. Rev. B* **2014**, *90*, 094102. [CrossRef]
4. Flamant, Q.; Gurak, M.; Clarke, D.R. The effect of zirconia substitution on the high-temperature transformation of the monoclinic-prime phase in yttrium tantalate. *J. Eur. Cera. Soc.* **2018**, *38*, 3925–3931. [CrossRef]
5. Virkar, A.V. Role of Ferroelasticity in toughening of zirconia ceramics. *Key Eng. Mater.* **1998**, *153–154*, 183–210. [CrossRef]
6. Zhang, F.; Zhang, G.J.; Yang, L.; Zhou, Y.C.; Du, Y. Thermodynamic modeling of $YO_{1.5}$-$TaO_{2.5}$ system and the effects of elastic strain energy and diffusion on phase transformation of $YTaO_4$. *J. Eur. Ceram. Soc.* **2019**, *39*, 5036–5047. [CrossRef]
7. Brixner, L.H.; Chen, H.Y. On the structural and luminescent properties of the M′-$LnTaO_4$ rare-earth tantalates. *J. Electrochem. Soc.* **1983**, *130*, 2435–2443. [CrossRef]
8. Wang, J.; Yu, X.; Zhou, C.R.; Feng, J. Microstructure and thermal properties of $RETaO_4$ (RE = Nd, Eu, Gd, Dy, Er, Yb, Lu) as promising thermal barrier coating materials. *Scr. Mater.* **2017**, *126*, 24–28. [CrossRef]
9. Chen, L.; Wang, J.; Feng, J. Research progress of rare earth tantalate ceramics as thermal barrier coatings. *Sci. China Mater.* **2017**, *36*, 938–949.
10. Zhu, J.T.; Lou, Z.H.; Zhang, P.; Zhao, J.; Meng, X.Y.; Xu, J.; Gao, F. Preparation and thermal properties of rare earth tantalates ($RETaO_4$) high-entropy ceramics. *J. Inorg. Mater.* **2021**, *36*, 411–417. [CrossRef]

11. Kresse, G.; Furthmüller, J. Efficient iterative schemes for ab initio total-energy calculations using a plane-wave basis set. *Phys. Rev. B* **1996**, *54*, 11169–11186. [CrossRef] [PubMed]
12. Kresse, G.; Furthmüller, J. Efficiency of ab initio total energy calculations for metals and semiconductors using a planewave basis set. *Comp. Mater. Sci.* **1996**, *6*, 15–50. [CrossRef]
13. Blöchl, P.E. Projector augmented-wave method. *Phys. Rev. B* **1994**, *50*, 17953–17979. [CrossRef] [PubMed]
14. Perdew, J.P.; Burke, K.; Ernzerhof, M. Generalized gradient approximation made simple. *Phys. Rev. Lett.* **1996**, *77*, 3865–3868. [CrossRef]
15. Blöchl, P.E.; Jepsen, O.; Andersen, O.K. Mproved tetrahedron method for brillouin-zone integrations. *Phys. Rev. B* **1994**, *49*, 16223–16233. [CrossRef] [PubMed]
16. Landau, L.D.; Lifshitz, E.M. *Theory of Elasticity Butterworth*; Heinemann: Oxford, UK, 1999.
17. Voigt, W. *Lehrburch der Kristallphysik*; Teubner: Leipzig, Germany, 1928.
18. Reuss, A. Calculation of flow limits of mixed crystals on the basis of plasticity of single crystals. *Z. Angew. Math. Mech.* **1929**, *9*, 49–58. [CrossRef]
19. Hill, R. The elastic behaviour of a crystalline aggregate. *Proc. Phys. Soc. Sect. A* **1952**, *65*, 349–354. [CrossRef]
20. Sych, A.B.; Golub, M. Niobates and tantalates of tervalent elements. *Russ. Chem. Rev.* **1977**, *46*, 210. [CrossRef]
21. Hartenbach, I.; Lissner, F.; Nikelski, T.; Meier, S.F.; Müller-Bunz, H.; Schleid, T. Über oxotantalate der lanthanide des formeltyps $MTaO_4$ (M = La–Nd, Sm–Lu). *Z. Anorg. Allg. Chem.* **2005**, *631*, 2377–2382. [CrossRef]
22. Mather, S.A.; Davies, P.K. Nonequilirbium phase formation in oxides prepared at low temperature: Fergusonite-related phases. *J. Am. Ceram. Soc.* **1995**, *78*, 2737–2745. [CrossRef]
23. Zhang, F.; Wang, J.C.; Liu, S.H.; Du, Y. Effects of the volume changes and elastic-strain energies on the phase transition in the Li-Sn battery. *J. Power Sources* **2016**, *330*, 111–119. [CrossRef]
24. Stubičan, V.S. High-temperature transitions in rare-earth niobates and tantalates. *J. Am. Ceram. Soc.* **1964**, *47*, 55–58. [CrossRef]
25. Watt, J.P.; Peselnick, L. Clarification of the hashine shtrikman bounds on the effective elastic moduli of polycrystals with hexagonal, trigonal, and tetragonal symmetries. *J. Appl. Phys.* **1980**, *51*, 1525–1531. [CrossRef]
26. Söderlind, P.; Klepeis, J.E. First-principles elastic properties of α-Pu. *Phys. Rev. B* **2009**, *79*, 104110. [CrossRef]
27. Born, M. On the stability of crystals. *Proc. Camb. Philos. Soc.* **1940**, *36*, 160. [CrossRef]
28. Pugh, S.F. XCII. Relations between the elastic moduli and the plastic properties of polycrystalline pure metals. *Lond. Edinb. Dublin Philos. Mag. J. Sci.* **1954**, *45*, 823–843. [CrossRef]
29. Wei, N.; Zhang, X.L.; Zhang, C.G.; Hou, S.J.; Zeng, Z. First-principles investigations on the elastic and thermodynamic properties of cubic ZrO2 under high pressure. *Int. J. Mod. Phy. C* **2015**, *26*, 1550056. [CrossRef]
30. Chen, X.Q.; Niu, H.; Li, D.; Li, Y. Modeling hardness of polycrystalline materials and bulk metallic glasses. *Intermetallics* **2011**, *19*, 1275–1281. [CrossRef]
31. Tian, Y.; Xu, B.; Zhao, Z. Microscopic theory of hardness and design of novel superhard crystals. *J. Meta. Hard Mater.* **2012**, *33*, 93–106. [CrossRef]
32. Ranganathan, S.I.; Ostoja-Starzewski, M. Universal Elastic Anisotropy Index. M. *Phys. Rev. Lett.* **2008**, *101*, 055504. [CrossRef] [PubMed]